Article

On the Nature of Antimicrobial Activity: A Model for Protegrin-1 Pores

Allison A. Langham, Abdallah Sayyed Ahmad, and Yiannis N. Kaznessis

J. Am. Chem. Soc., **2008**, 130 (13), 4338-4346 • DOI: 10.1021/ja0780380

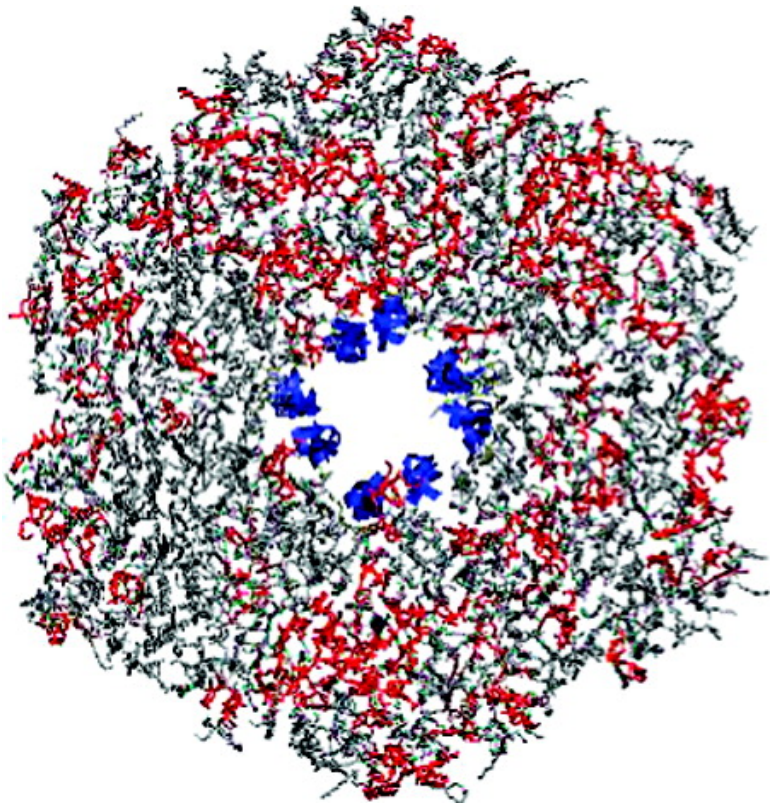

J|A|C|S
ARTICLES
Published on Web 03/12/2008

On the Nature of Antimicrobial Activity: A Model for Protegrin-1 Pores

Allison A. Langham, Abdallah Sayyed Ahmad, and Yiannis N. Kaznessis*

Department of Chemical Engineering and Materials Science, 421 Washington Avenue SE, Minneapolis, Minnesota 55455

Received October 19, 2007; E-mail: yiannis@cems.umn.edu

Abstract: We conducted over 150 ns of simulation of a protegrin-1 octamer pore in a lipid bilayer composed of palmitoyloleoyl-phosphatidylethanolamine (POPE) and palmitoyloleoyl-phosphatidylglycerol (POPG) lipids mimicking the inner membrane of a bacterial cell. The simulations improve on a model of a pore proposed from recent NMR experiments and provide a coherent understanding of the molecular mechanism of antimicrobial activity. Although lipids tilt somewhat toward the peptides, the simulated protegrin-1 pore more closely follows the barrel-stave model than the toroidal-pore model. The movement of ions is investigated through the pore. The pore selectively allows negatively charged chloride ions to pass through at an average rate of one ion every two nanoseconds. Only two events are observed of sodium ions crossing through the pore. The potential of mean force is calculated for the water and both ion types. It is determined that the chloride ions move through the pore with ease, similarly to the water molecules with the exception of a zone of restricted movement midway through the pore. In bacteria, ions moving through the pore will compromise the integrity of the transmembrane potential. Without the transmembrane potential as a countermeasure, water will readily flow inside the higher osmolality cytoplasm. We determine that the diffusivity of water through a single PG-1 pore is sufficient to cause fast cell death by osmotic lysis.

Introduction

Antimicrobial peptides (AMPs) have long been considered as a potential alternative antibiotic treatment. AMPs are typically small, cationic peptides that are part of the innate immune response of most plants, insects and animals.[1] They are believed to defend the host by selectively destroying the microbial cell wall, although the mechanism of action through which this occurs is not fully understood.

An important hypothesis is that multiple peptides form aggregates that work against the microbial cell membrane, either by the barrel-stave or toroidal pore mechanism or the carpet mechanism (see Brogden's review for a recent discussion of the differences between the mechanisms).[2] Briefly, the carpet model indicates surface bonding of the peptide to the cell membrane, while the toroidal pore and barrel-stave models are two types of peptide transmembrane pores differentiated by the lipid orientation near the peptides. Due to difficulties in the use of traditional experimental methods on lipid bilayer systems, the determination of the aggregated structures of AMPs is rare. Recently, the aggregated structures of protegrin-1 (PG-1) in palmitoyloleoyl-phosphatidylethanolamine:palmitoyloleoyl-phosphatidylglycerol (POPE:POPG) and palmitoyloleoyl-phosphocholine (POPC):cholesterol bilayers were determined.[3] Mani and co-workers observed that the peptides aggregate on the surface of the mammalian membrane mimicking the POPC:cholesterol bilayer, while they permeate the negatively charged bacterial membrane mimicking the POPE:POPG bilayer. On the basis of distance constraints, they proposed that PG-1 forms an octameric pore structure in the latter type of bilayer. The protegrins are a family of five potent, naturally occurring, cationic antimicrobial peptides that were originally purified from porcine tissue.[4,5] Protegrin-1 [PG-1, RGGRL CYCRR RFCVC VGR] can launch a rapid response to infection by diverse bacterial species[6] including *Escherichia coli*, *Candida albicans*, and *Listeria monocytogenes*.[4,6] The NMR study by Mani and co-workers has provided an improved understanding of the insertion of the peptides into the two types of membranes. Nonetheless, their model remains a crude one lacking unambiguous atomistic level resolution. Specifically, the pore structure stability, the structure of the lipid membrane around the pore and the ion movement through the pore remain unresolved. These are important pieces of the puzzle that will help in revealing the molecular mechanism of action of antimicrobial peptides.

(1) Zasloff, M. Antimicrobial peptides of multicellular organisms. *Nature* **2002**, *415*, 389−395.
(2) Brogden, K. A. Antimicrobial peptides: pore formers or metabolic inhibitors in bacteria. *Nat. Rev. Microbiol.* **2005**, *3*, 238−250.
(3) Mani, R.; Tang, M.; Wu, X.; Buffy, J. J.; Waring, A. J.; Sherman, M. A.; Hong, M. Membrane-bound dimer structure of a beta-hairpin antimicrobial peptide from rotational-echo double-resonance solid-state NMR. *Biochemistry* **2006**, *45*, 8341−8349.
(4) Kokryakov, V. N.; Harwig, S. S.; Panyutich, E. A.; Shevchenko, A. A.; Aleshina, G. M.; Shamova, O. V.; Korneva, H. A.; Lehrer, R. I. Protegrins: leukocyte antimicrobial peptides that combine features of corticostatic defensins and tachyplesins. *FEBS Lett.* **1993**, *327*, 231−236.
(5) Qu, X. D.; Harwig, S. S.; Shafer, W. M.; Lehrer, R. I. Protegrin structure and activity against Neisseria gonorrhoeae. *Infect. Immun.* **1997**, *65*, 636−639.
(6) Drin, G.; Temsamani, J. Translocation of protegrin I through phospholipid membranes: role of peptide folding. *Biochim. Biophys. Acta* **2002**, *1559*, 160−170.

10.1021/ja0780380 CCC: $40.75

While molecular dynamics (MD) simulations can provide a detailed picture of the interactions between peptides and model membranes,[7−23] their use is still limited due to the long time scales required to observe aggregation and penetration of the bilayer by AMPs. The pore structure of PG-1 in a mixed POPE:POPG bilayer that was predicted from NMR experiments can, however, be used as a starting configuration for MD simulations of the pore system, allowing a molecular level view of the interactions between the pore and the bilayer system. In this work we present the results of over 150 ns of simulation of a PG-1 pore in a large lipid bilayer patch composed of 432 lipids. The entire system was solvated in nearly 14,000 water molecules with an additional sodium chloride concentration of 0.15 M (Figure 1). We performed over 50 ns of NP_ZAT simulation followed by over 100 ns of NPT simulation of the PG-1 pore in a POPE:POPG bilayer. The results from the simulations provide insight into the molecular mechanism of antimicrobial activity. In what follows we discuss the results of the simulation and propose a means by which PG-1 kills bacteria. We determine that the pore has a barrel-stave rather than a toroidal structure, and predict that the fast transport of water through the pore can lead to bacterial cell death due to osmotic lysis.

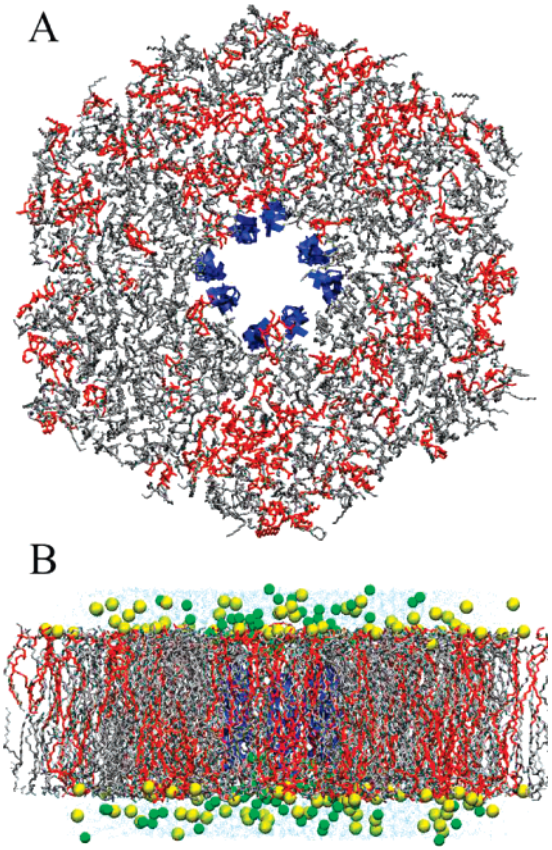

Figure 1. Initial views of the system. In A, the pore system is shown from the top, with protein in blue, POPE in gray, and POPG in red. In B, a side view is shown, with water in cyan, and chloride and sodium ions in yellow and green, respectively.

Experimental Procedures

System Construction. The structure of the pore was obtained from Professor Hong and co-workers, who constructed the model using Insight II as described in ref 3. To construct the lipid bilayer, we followed the method outlined by Roux and co-workers.[23−26] As the libraries provided for use with this method consist of DPPC molecules, we obtained a smaller library of POPC lipids from Professor Feller's website (persweb.wabash.edu/facstaff/fellers/). Each phosphatidylcholine head group was then replaced with a phosphatidylethanolamine group. The bilayer was constructed initially out of all POPE lipids. The number of core atom overlaps was reduced through systematic rigid body rotations and translations. One out of every four POPE lipids was selected at random and replaced with a POPG lipid to result in a system with a 3:1 POPE:POPG ratio. Each leaflet contained 216 lipids with the fatty acid chains of both leaflets pointing toward the center of the simulation cell, and each leaflet was hydrated by a layer of TIP3P water molecules approximately 10 Å thick. Sodium counterions were added near each POPG head group and chloride ions were added to neutralize the charge of the peptides. An additional concentration of 0.15 M of sodium chloride was added at this point. The system was constructed in a hexagonal cell with the *z*-axis perpendicular to the hexagonal face. Since the area per lipid for a 3:1 POPE:POPG membrane has not been experimentally determined, the simulation cell

(7) Bolintineanu, D., et al. Molecular dynamics simulations of three protegrin-type anti-microbial peptides: interplay between charges at the termini, β-sheet structure and amphiphilic interactions. *Mol. Simul.* **2007**, *33*, 809−819.
(8) Khandelia, H.; Kaznessis, Y. Cation-π Interactions Stabilize the Structure of the Antimicrobial Peptide Indolicidin near Membranes: Molecular Dynamics Simulations. *J. Phys. Chem. B* **2007**, *111* (1), 242−250.
(9) Khandelia, H.; Kaznessis, Y. N. Molecular dynamics investigation of the influence of anionic and zwitterionic interfaces on antimicrobial peptides' structure: Implications for peptide toxicity and activity. *Peptides* **2006**, *27*, 1192−200.
(10) Khandelia, H.; Kaznessis, Y. N. Molecular dynamics simulations of helical antimicrobial peptides in SDS micelles: what do point mutations achieve. *Peptides* **2005**, *26*, 2037−2049.
(11) Khandelia, H.; Kaznessis, Y. N. Structure of the antimicrobial beta-hairpin peptide protegrin-1 in a DLPC lipid bilayer investigated by molecular dynamics simulation. *Biochim. Biophys. Acta* **2007**, *1768*, 509−520.
(12) Khandelia, H.; Kaznessis, Y. N. Molecular dynamics simulations of the helical antimicrobial peptide ovispirin-1 in a zwitterionic dodecylphosphocholine micelle: insights into host-cell toxicity. *J. Phys. Chem. B* **2005**, *109*, 12990−12996.
(13) Khandelia, H.; Langham, A. A.; Kaznessis, Y. N. Driving engineering of novel antimicrobial peptides from simulations of peptide-micelle interactions. *Biochim. Biophys. Acta* **2006**, *1758*, 1224−1234.
(14) Langham, A.; Kaznessis, Y. Effects of mutations on the C-terminus of Protegrin-1: A molecular dynamics simulation study. *Mol. Simul.* **2006**, *32*, 193−201.
(15) Langham, A. A.; Khandelia, H.; Kaznessis, Y. N. How can a beta-sheet peptide be both a potent antimicrobial and harmfully toxic? Molecular dynamics simulations of protegrin-1 in micelles. *Biopolymers* **2006**, *84*, 219−231.
(16) Langham, A. A.; Waring, A. J.; Kaznessis, Y. N. Comparison of interactions between β-hairpin decapeptides and SDS/DPC micelles from experimental and simulation data. *BMC Biochem.* **2007**, *8*, 11.
(17) Ostberg, N.; Kaznessis, Y. Protegrin structure-activity relationships: using homology models of synthetic sequences to determine structural characteristics important for activity. *Peptides* **2005**, *26*, 297−306.
(18) Shental-Bechor, D.; Haliloglu, T.; Ben-Tal, N. Interactions of cationic-hydrophobic peptides with lipid bilayers: a Monte Carlo simulation method. *Biophys J.* **2007**, *93* (6), 1858−1871.
(19) Hsu, J. C.; Yip, C. M. Molecular dynamics simulations of indolicidin association with model lipid bilayers. *Biophys J.* **2007**, *92* (12), L100−102.
(20) Leontiadou, H.; Mark, A. E.; Marrink, S. J. Antimicrobial peptides in action. *J Am Chem. Soc.* **2006**, *128* (37), 12156−12161.
(21) Jang, H.; Ma, B.; Woolf, T. B.; Nussinov, R. Interaction of protegrin-1 with lipid bilayers: membrane thinning effect. *Biophys J.* **2006**, *91* (8), 2848−2859.
(22) Aliste, M. P.; Tieleman, D. P. Computer simulation of partitioning of ten pentapeptides Ace-WLXLL at the cyclohexane/water and phospholipid/water interfaces. *BMC Biochem.* **2005**, *6*, 30.
(23) Berneche, S.; Nina, M.; Roux, B. Molecular dynamics simulation of melittin in a dimyristoylphosphatidylcholine bilayer membrane. *Biophys J* **1998**, *75*, 1603−1618.
(24) Berneche, S.; Roux, B. Molecular dynamics of the KcsA K(+) channel in a bilayer membrane. *Biophys J* **2000**, *78*, 2900−2917.
(25) Woolf, T. B.; Roux, B. Structure, energetics, and dynamics of lipid-protein interactions: A molecular dynamics study of the gramicidin A channel in a DMPC bilayer. *Proteins* **1996**, *24*, 92−114.
(26) Woolf, T. B.; Roux, B. Molecular dynamics simulation of the gramicidin channel in a phospholipid bilayer. *Proc. Natl. Acad Sci. U.S.A.* **1994**, *91*, 11631−11635.

dimensions were initially set to allow for an area per lipid of 61.5 Å^2/lipid, as reported by Rog and co-workers.[27]

Minimization and Production. The system was minimized using CHARMM version c30b2 with the charmm27 parameter set. Harmonic constraints were initially placed on the lipids to prevent penetration of water into the bilayer and cylindrical harmonic constraints were placed on the peptides to prevent the pore structure from collapsing. Electrostatic interactions were calculated using the particle mesh Ewald summation with grid points approximately 1 Å apart in each direction, a β-spline order of 4 and real space Gaussian width of 0.32 as described in ref 11. The nonbonded van der Waals forces were smoothly switched off between 8 and 11 Å. The system was minimized for 2000 steps through alternating sets of 500 steps of adopted basis Newton−Raphson (ABNR) and steepest descent (SD) minimizations. SHAKE was then applied to eliminate the fastest degrees of freedom involving bonds with hydrogen atoms. An additional 2500 total steps of ABNR and SD minimization were performed. At this point the simulation was transferred to the better scalable simulation engine NAMD.[28] Similarly, electrostatic interactions were treated with PME with a grid of approximately 1 point per Å. Nonbonded van der Waals interactions were smoothly switched over 3 Å between 8 and 11 Å. The Nosé-Hoover Langevin piston [29,30] was used for pressure control with a piston period set to 200 fs and piston decay of 100 fs. The system was minimized for 5000 steps and then heated to 310 K in increments of 30 K, minimizing for 5000 steps at each temperature. The area of the hexagonal simulation cell was constrained to a constant value (using the ConstantArea function in NAMD) for the first 50 ns of simulation.

After 50 ns of simulation at constant area, the system was switched to the NPT ensemble, employing the ConstantRatio function in NAMD to keep the ratio of the x and y dimensions of the cell constant. The simulation was continued for an additional 100 ns, at which point a constant area per lipid had been observed for more 30 ns. There is an ongoing debate in the literature about the adequate thermodynamic ensemble for lipid bilayer simulations.[31−33] Although the NPT (constant number of atoms, pressure and temperature) ensemble is used in most biomolecular MD simulations, problems with the area per lipid may arise for lipid bilayer simulations. This is particularly true for simulations using CHARMM, for which NP$_z$AT or NPγT ensembles are typically recommended, where either the $x-y$ plane area or the surface tension are held constant but the z dimension, normal to the bilayer, is allowed to fluctuate to retain constant pressure. In the bilayer simulations that have been presented in the literature, the simulation cell in NPT simulations using CHARMM or NAMD regularly shrinks, reducing the area per lipid. Jensen and co-workers simulated a lipid bilayer containing 36 DPPC lipids per leaflet in the NPT ensemble and observed the $x-y$ dimensions of the cell decrease for the entire 15 ns simulation.[34] The system undergoes an unrealistic expansion of the lipids in the z-direction, such that the two leaflets have separated. Feller and Pastor explained the unnatural behavior of lipid bilayers in simulations as an artifact due to the small sizes of the simulated systems.[31] Long wavelength undulations of the bilayer are absent in small simulation cells, causing an increase in the surface tension over what would normally be expected from a macroscopic bilayer. In our simulations, we have carefully monitored the bilayer properties throughout the simulation and believe that using a larger bilayer has allowed us to avoid the problems seen by Jensen and co-workers. We thus recommend that lipid bilayer simulations be conducted with at least 200 lipids per leaflet. A systematic study of the influence of the system's size on its stability would be of interest but is beyond the scope of the current study.

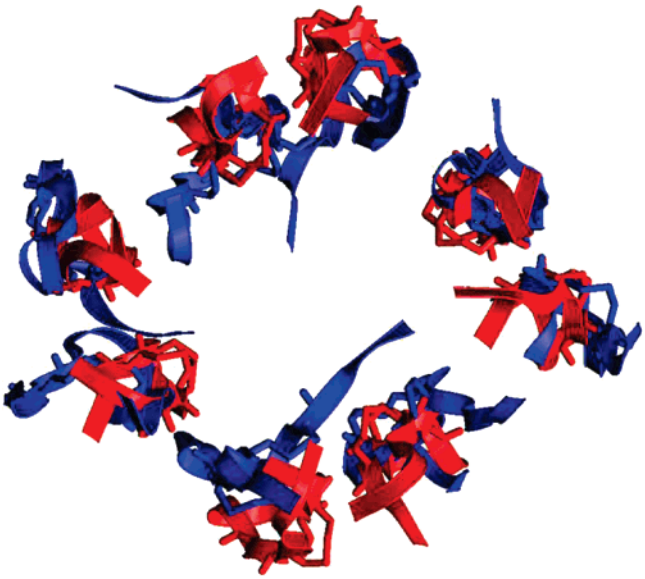

Figure 2. Overlay of the initial (red) and final (blue) structures of the pore. Little difference is observed in the positioning of the peptides into a group of four dimers, although differences in the individual peptide structures are noted, particularly at the N-termini. Please see Supporting Information for more data regarding the stability of the pore structure.

Results

Comparing the pore structure initially proposed by Mani and co-workers in ref 3 to the final structure after more than 150 ns of simulation, we find little difference in the overall structure (Figure 2). Using an inner radius from the center of the pore to the first peptide atom projected on the $x-y$ plane, the opening of the pore has an area of nearly 400 Å^2; a maximum predicted pore area of 1385 Å^2 includes the area taken up by the width of the peptides themselves. The area of pore approximates these dimensions throughout the simulation (plot in Supporting Information).

More specifically, the peptides remain grouped into an assembly of four dimers, with the dimer structures still intact. There are differences in the positions of the N-terminal strands, consistent with the flexibility of this part of the peptide. The distances between phenylalanine residues for dimer pairs remain relatively constant throughout the simulation, as do distances between tyrosine residues on interdimer pairs. Please see Supporting Information for a more detailed discussion of the stability of the pore.

Bilayer Thickness and Lipid Tilt. Molecular dynamics simulations provide an opportunity to study the impact of the pore on the lipid structure, behavior and organization. One property that can be used to quantify the impact is bilayer thickness as a function of radial distance outward from the pore center. Membrane thinning is apparent with the thickness

(27) Rog, T.; Murzyn, K.; Pasenkiewicz-Gierula, M. Molecular dynamics simulations of charged and neutral lipid bilayers: treatment of electrostatic interactions. *Acta Biochim. Pol.* **2003**, *50*, 789−798.
(28) Phillips, J. C.; Braun, R.; Wang, W.; Gumbart, J.; Emad, T.; Villa, E.; Chipot, C.; Skeel, R. D.; Kale, L.; Schulten, K. Scalable molecular dynamics with NAMD. *J. Comput. Chem.* **2005**, *26*, 1781−1802.
(29) Feller, S. E.; Zhang, Y.; Pastor, R. W.; Brooks, B. R. Constant pressure molecular dynamics simulation: The Langevin piston method. *J. Chem. Phys.* **1995**, *103*, 4613−4621.
(30) Martyna, G. J.; Tobias, D. J.; Klein, M. L. Constant pressure molecular dynamics algorithms. *J. Chem. Phys.* **1994**, *101*, 4177−4189.
(31) Feller, S. E.; Pastor, R. W. On simulating lipid bilayers with an applied surface tension: periodic boundary conditions and undulations. *Biophys. J.* **1996**, *71*, 1350−1355.
(32) Jahnig, F. What is the surface tension of a lipid bilayer membrane. *Biophys. J.* **1996**, *71*, 1348−1349.
(33) Roux, B. Commentary: surface tension of biomembranes. *Biophys. J.* **1996**, *71*, 1346−1347.
(34) Jensen, M. O.; Mouritsen, O. G.; Peters, G. H. Simulations of a membrane-anchored peptide: structure, dynamics, and influence on bilayer properties. *Biophys. J.* **2004**, *86*, 3556−3575.

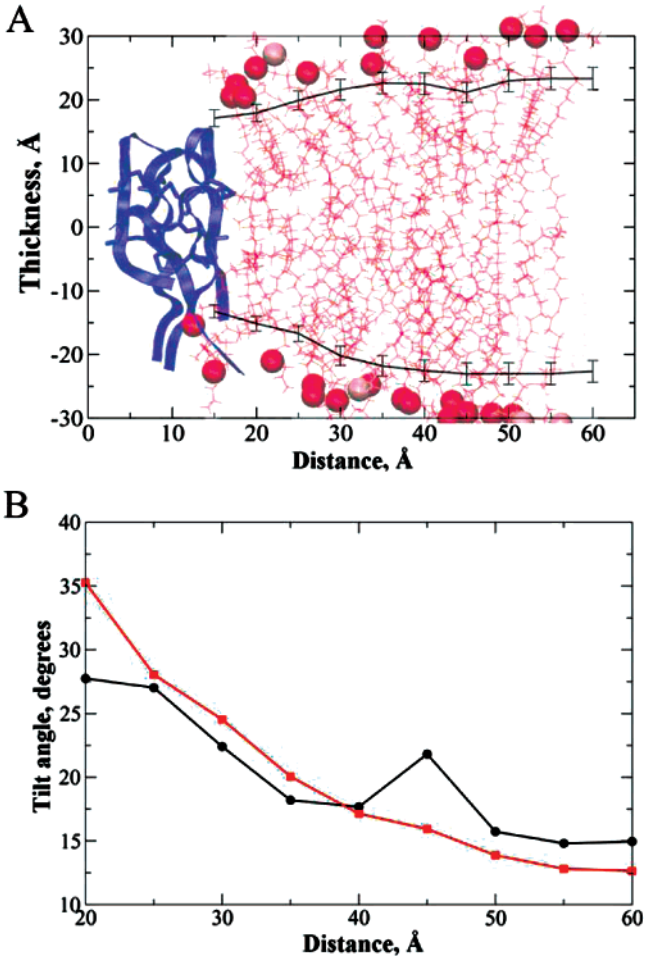

Figure 3. Average thickness of the bilayer as a function of distance from the pore (averaged over the last 30 ns of simulation). The bilayer thins near the pore to allow for the mismatch in heights of the lipid compared to height of the peptide. At the bottom is lipid tilt angle as a function of the distance from the center pore for upper leaflet lipids (black) and lower leaflet lipids (red).

decreasing from 45 to 50 Å away from the pore to around 35 Å at the pore. As seen in Figure 3, the lipids clearly reorient themselves near the pore. The lipids closest to the pore tilt away from the bilayer normal to allow the phosphate groups to interact with the positively charged arginines at both the termini and turn regions of the peptides. This tilting allows for the thinning of the bilayer region close to the pore.

Ion Transport. Another aspect of the pore that can be explored through MD simulations is the movement of ions through the pore. The chloride counterions were observed to move quickly and with high frequency into and out of the pore. Shown in Figure 4 are plots of the *z* coordinates of representative chloride and sodium ions with respect to time. The sodium ion (Figure 4B) vacillates near the membrane, and occasionally passes through the periodic boundary conditions (figures shown are based on unfolded trajectories). The chloride ion (Figure 4A) moves similarly until 75 ns into the simulation, when it passes through the pore. Overall, we see the chloride ions entering and exiting the pore with much greater frequency than the sodium ions. We observe over 300 events in which chloride ions enter the pore; they traverse the pore 55 times during the 100 ns of NPT simulation, while in the remaining events the ions enter and exit on the same side. This is contrasted with only two events in which sodium ions travel through the pore

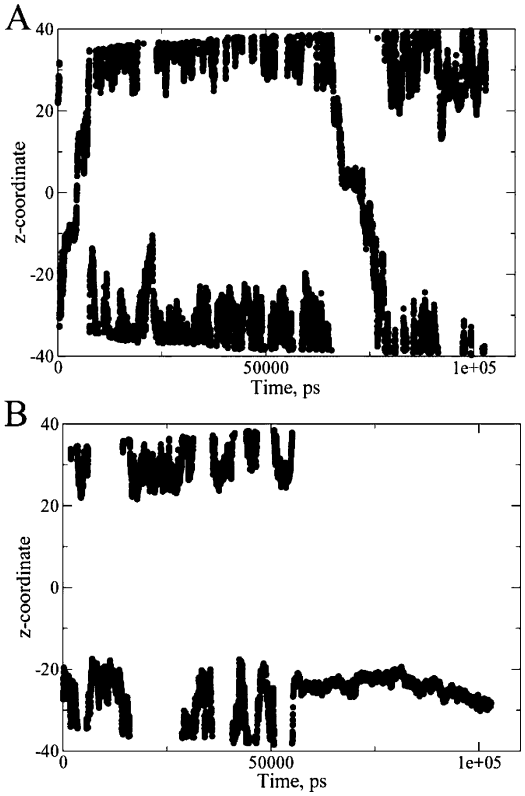

Figure 4. Time profiles of the *z*-coordinate of representative chloride (A) and sodium (B) ions. We see 55 events of chloride ions crossing through the pore during the entire simulation, one of which is shown in (A). Only two sodium ions cross through the pore, one of which is shown in (B).

during the same period of time. There appears to be no strong preference for direction of travel through the pore in the absence of transmembrane potential and concentration gradients, with ions moving from the negative *z*-direction to the positive one 31 times and from positive to negative 24 times. If this 25% difference is taken to be more than statistical fluctuation, the simulation predicts a slight preference for ions moving through the bilayer from the side of the pore at the turn of the β-hairpins to the termini side. In a real cellular system, this effect may become more pronounced due to the effects the movement of the ions would have on the electrostatic potential across the membrane; however, due to the periodic boundary conditions used in the simulation, there is no ion concentration gradient in the simulation.

The pore is large enough to accommodate multiple ions at any one point in time. On average, the chloride ions that cross through the pore require approximately 10 ns to move from one side of the bilayer to the other. For chloride ions that enter and exit the pore on the same side of the bilayer (those that do not cross through), the average time spent in the pore is 5.4 ns, with a range from less than one to over 45 ns, usually spending around 2 ns in the pore. Please see the Supporting Information for a discussion of the ion residence time distribution. Figure 5 shows a plot of the chloride and sodium ion occupancy of the pore, clearly demonstrating the pore's preference for negatively charged ions. On average, there are 12 chloride ions in the pore at any given time during the simulation, contrasted with an average of less than one sodium ion. This is not unexpected, due to the strongly cationic nature of the pore. PG-1 has six arginines, mostly concentrated at the termini and turn region of the peptide, in addition to an amidated C-terminus. The

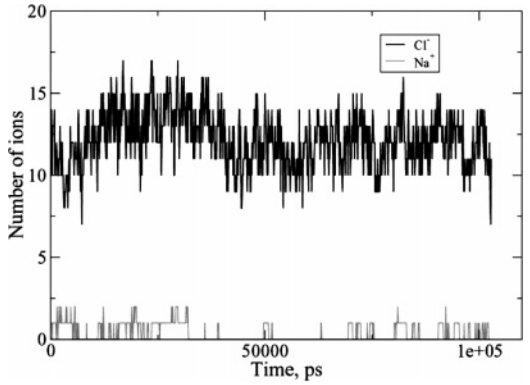

Figure 5. Pore ion occupancy. The numbers of each type of ion in the core of the pore were calculated through time.

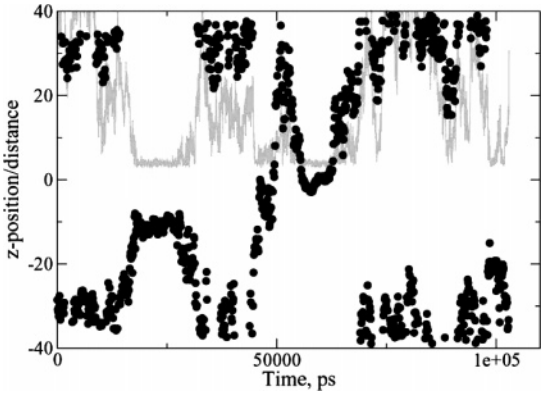

Figure 6. Position of a chloride ion in the *z*-direction (in black) and distance between the ion and the closest arginine side chain (in grey).

chloride ions are attracted to and associate with these positively charged residues. When the ions approach the pore, they often interact with an arginine residue. In some cases, as in the time interval from 20 to 30 ns and again from 55 to 65 ns in Figure 5, the chloride ion becomes electrostatically bound to its location near either the turn or the termini entrance of the pore. Thermal fluctuations eventually cause the ion to escape the pore most often from the same side it entered. For the ion in Figure 6, we see that at around 40 ns the ion again approaches the pore; this time it does not become as strongly associated with an arginine residue, allowing it to pass through the pore in less than 5 ns. The arginine residues clearly play an important role in keeping the pore open: these positively charged residues are more hydrophilic than the other residues in protegrin, and their presence prevents the pore from collapsing as a consequence of hydrophobic effects and the lateral pressure from the lipid molecules.

Potential of Mean Force Calculations. The equilibrium potential of mean force (PMF), *w*, which describes the governing force of ion and water permeation across the PG-1 pore, is related to the equilibrium number density, $c(\vec{r})$, and the average bulk density, $\bar{c}^{\infty}$, within the reference state far from the pore through the following [35−38]

$$\Delta w(\vec{r}) = w(\vec{r}) - w' = -k_B T \ln \frac{c(\vec{r})}{\bar{c}^{\infty}} \qquad (1)$$

where k_B is the Boltzmann constant, T is the temperature and the PMF affecting the behavior and mobility of ions or water molecules at the bulk reference state; w' is a constant with unassigned value. The difference between the potential of mean force affecting an ion or water molecule at the point $\vec{r}$ and the bulk region $\Delta w(\vec{r})$ can be directly computed from unbiased MD simulation trajectories, provided that sufficient sampling has been achieved during the MD simulation. The relatively fast movement of water molecules and chloride ions across the pore combined with the length of the simulation in the current study allow the accurate estimation of various properties of both chloride ions and water molecules in the pore region. The large number of ions included explicitly in the present simulation system also facilitates the production of statistically significant chloride ion PMF values.

The axisymmetric two-dimensional (2D) PMF of water, shown in Figure 7A, indicates that the region accessible to water molecules is approximately a cylinder with a radius of 10 Å and a density close to the bulk water density. This suggests that water molecules move relatively freely through the center of the pore, which is expected since the PG-1 pore is wide with more than 35 Å in diameter. Figure 7A also indicates that water molecules interact with the lipid headgroup region and often reach the periphery of the hydrophobic core. Furthermore, water molecules have a tendency to avoid the center of the pore on the turn side due to their attraction to the pore lining which is rich with charged arginine residues.

The PMF values for the chloride ions within the pore (Figure 7B) are similar to bulk water PMF values except that some regions near the turn side entrance of the pore are up to 2 kcal/mol lower than in the bulk region. A constriction zone with a barrier of roughly 1−2 kcal/mol can also be distinguished in the region: -6 Å $< z <$ 2 Å, indicating that chloride ions go through a bottleneck with a radius of approximately 10 Å. The 2D PMF for sodium ions, however, shows inadequate sampling due to the fact that there were just two sodium ion transitions through the pore observed during the NPT MD simulation (results not shown).

To study ion−ion correlations and ion pairings effects on ion transport across the pore, we calculated the average number of chloride ions located within 4.6 Å of the first chloride contact shell around sodium as a function of the distance along the axis of the pore. The number of chloride ions around each sodium ion in the first shell is significantly lower in the bulk region than that at the turn side entrance and the termini side of the pore (Figure 8), which suggests that screening effects may play an important role in facilitating such a passage, whereby a sodium ion will be shielded from electrostatic repulsions with the arginine residues as it crosses the pore.

Diffusion Coefficient Calculations. The diffusional mobility of water and ions in the bulk and within the pore can be measured by the diffusion coefficient, *D*, which can be obtained from the slope of mean square displacement versus time. Specifically, we compute the spatial distribution of the local

(35) Beckstein, O.; Tai, K.; Sansom, M. S. P. Not Ions Alone: Barriers to Ion Permeation in Nanopores and Channels. *J. Am. Chem. Soc.* **2004**, *126*, 14694−14695.
(36) Leontiadou, H.; Mark, A. E.; Marrink, S. J. Ion transport across transmembrane pores. *Biophys. J.* **2007**, *92*, 4209−4215.
(37) Roux, B.; Allen, T.; Berneche, S.; Im, W. Theoretical and computational models of biological ion channels. *Q. Rev. Biophys.* **2004**, *37*, 15−103.
(38) Leontiadou, H.; Mark, A. E.; Marrink, S.-J. Ion Transport across Transmembrane Pores. *Biophys. J.* **2007**, *92*, 4209−4215.

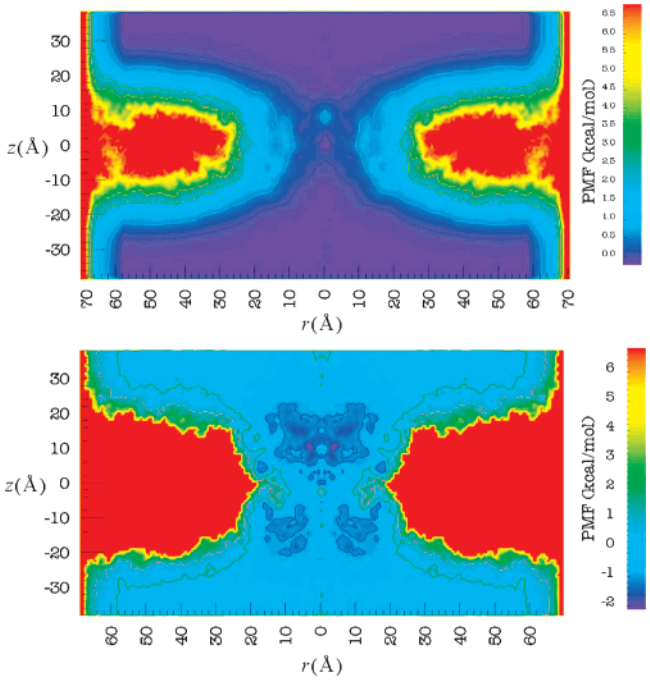

Figure 7. (Top) 2D PMF of a single water molecule as a function of the distance from and the position along the axis of the pore (r,z). The contour lines are drawn at 0.0, 0.5, 1.0, 2.0, and 3.0 kcal/mol. The map was constructed using the last 50 ns of the NPT simulation trajectory and 1 Å grid size. (Bottom) 2D PMF of a single chloride ion as a function of the distance from and the position along the axis of the pore (r,z). The contour lines are drawn at −1.0, 0.0, and 1.0 kcal/mol. The map was constructed using the last 50 ns of the NPT simulation trajectory and 1 Å grid size.

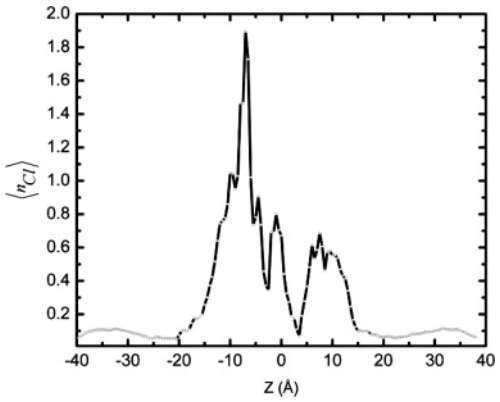

Figure 8. Average number of chloride ions in the first chloride ion shell around sodium ions as a function of the position along the axis of the pore. The histogram was constructed using the whole NPT simulation trajectory and 0.5 1 Å bin size.

diffusion coefficient at position $\vec{r}$ using the following finite difference expression[39,40]

$$D(\vec{r}) = \frac{1}{6\Delta t}\langle|\vec{r}_i(t_j + 2\Delta t) - \vec{r}_i(t_j)|^2 - |\vec{r}_i(t_j + \Delta t) - \vec{r}_i(t_j)|^2\rangle \quad (2)$$

where the angle brackets indicate an average over time and all solvent molecules or ions which are found to reside in the volume element around $\vec{r}$ at time t_j. The value of Δt was fixed at 1 ps. The choice of Δt is based on the assumption that water molecules and ions will not diffuse more than a few angstroms in 2 ps. This assumption is consistent with results from the current simulation. To reveal the effects of the pore on the diffusional mobility of solvent molecules and ions, we only consider the diffusion coefficient component parallel to the axis of the pore as a function of the radial distance from the center and position along the axis of the pore for water molecules ($D_{z,H2O}(r,z)$), and only as a function of position along the axis of the pore for chloride ions ($D_{z,Cl}(z)$). Analysis of the 2D diffusion coefficient for the chloride ion and the diffusion coefficient profile of sodium ion were both hindered by the significant noise in the data due to the relatively low sampling of ions. Figure 9A shows the 2D water diffusion coefficient of water molecules along the z-axis as a function of distance from the pore and position along the axis of the pore (r,z). The water diffusion coefficient map was constructed using the last 30 ns of the NPT simulation trajectory and a 1 Å grid size. The bulk value of the water diffusion coefficient is found to be close to the experimentally observed bulk diffusion coefficient of 0.23 Å^2/ps.[41] The contour lines drawn at 0.13 and 0.24 Å^2/ps indicate that water diffuses relatively easily along the axial direction as compared to bulk. However, the diffusion coefficient of water molecules decreases by up to 45% of its bulk value at the center of the pore, especially in the region -2Å $< z <$ 5Å.

Figure 9B demonstrates the diffusional mobility behavior of chloride ions along the axis of the pore. The diffusion coefficient in the bulk is calculated to be 0.12 Å^2/ps, which is an underestimate of the experimentally measured value of 0.18 Å^2/ps.[42] Despite the differences in the computed values of the diffusion coefficient of the chloride ions, it is expected that the observed variations relative to the bulk will still be qualitatively valid. Hence, the diffusion coefficient value of chloride ions is expected to be reduced to about 40% of its estimated bulk value at the narrowest part of the pore. There is also a spike in the diffusion coefficient of chloride ions around $z = -5$ Å, indicating that chloride ions diffuse more freely in that region.

Ion Conductance. In principle, calculating the ion conductance across an ion channel or a pore requires all-atom nonequilibrium MD simulations with applied transmembrane voltages. Nonetheless, at low voltages for near equilibrium cases, the effect of the transmembrane potential on ion permeation can be neglected. In such a case, the maximum conductance corresponding to ion transport under saturation conditions can be estimated using

$$g_{max} = \frac{q^2}{k_B T L_{pore}^2}\left(\frac{1}{L_{pore}}\int_0^{L_{pore}} dz/D(z)e^{-w(z)/k_B T}\right)^{-1}\left(\frac{1}{L_{pore}}\int_0^{L_{pore}} e^{-w(z)/k_B T}dz\right)^{-1} \quad (3)$$

where L_{pore} is the length of the pore and q is the charge of the permeating ion.[43] This approach yields a crude estimate of the conductance since it ignores the effects of multiple ion oc-

(39) Lounnas, V.; Pettitt, B. M.; Phillips, G. N., Jr. A global model of the protein-solvent interface. *Biophys. J.* **1994**, *66*, 601−614.
(40) Makarov, V. A.; Feig, M.; Andrews, B. K.; Pettitt, B. M. Diffusion of Solvent around Biomolecular Solutes: A Molecular Dynamics Simulation Study. *Biophys. J.* **1998**, *75*, 150−158.
(41) Hertz, H. G. Electron Resonance Relaxation Spectroscopy. In *In Water: A Comperhensive Treatise*; Franks, F., Ed.; Plenum Press, New York, 1973; pp 301−395.
(42) Mills, R.; Lobo, V. *Self-Diffusion Coefficient in Electrolyte Solutions*; Physical Sciences Data, Vol. 36; Elsevier: New York. 1989.
(43) Allen, T. W.; Andersen, O. S.; Roux, B. Molecular dynamics: potential of mean force calculations as a tool for understanding ion permeation and selectivity in narrow channels. *Biophys. Chem.* **2006**, *124*, 251−267.

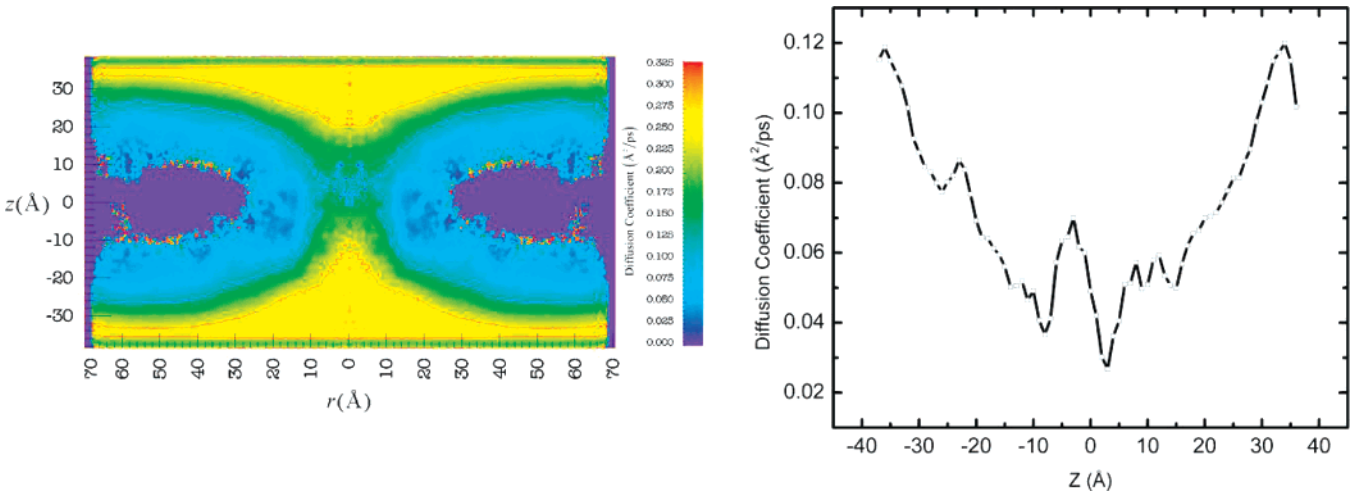

Figure 9. (Left) 2D water diffusion coefficient along the *z*-axis as a function of the distance from and the position along the axis of the pore (*r*,*z*). The contour lines are drawn at 0.13 and 0.24 Å²/ps. The water diffusion coefficient map was constructed using the last 50 ns of the NPT simulation trajectory and 1 Å grid size. (Right) The diffusion coefficient profile of chloride ions along the axis of the pore. The diffusion coefficient of chloride ions is reduced to about 40% of its bulk value. The chloride ion diffusion coefficient profile was constructed using the last 50 ns of the NPT simulation trajectory and 1 Å bin size.

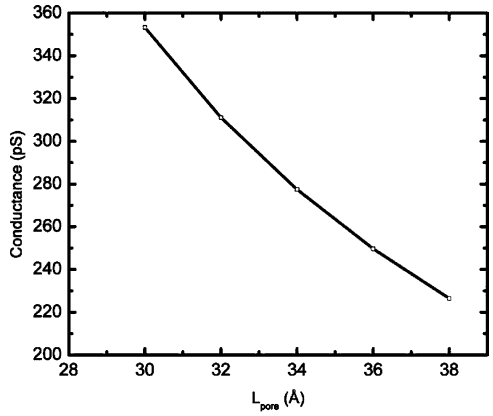

Figure 10. The maximum conductance of the PG-1 pore as a function of the assumed pore length.

cupancy on the permeation of ions across the pore. We calculate the maximum conductance for the pore assuming a length range between 30 and 38 Å using eq 3, the diffusion coefficient profile of chloride ions shown in Figure 2B and the 1D PMF of chloride ions (not shown). Figure 10 illustrates the maximum conductance as a function of the pore length. The maximum conductance range is found to be between 220 pS (picoSiemens) and 350 pS, depending on the assumed pore length

Discussion

We have presented the results from 150 ns of simulation of a PG-1 pore in a POPE:POPG bilayer that corroborates experimental data for the same system. The size and shape of the pore in the simulation are in close agreement with the structure predicted from NMR data, with the structure remaining remarkably stable over a long simulation. With a sound structural foundation, the simulation has the potential to capture an atomistic resolution picture of the biophysics of AMP pore formation. The hope is that such a clear physical picture will result in insights regarding the biological function of these peptides.

One of the main points of interest of this study is the opportunity it has provided to determine whether PG-1 forms a toroidal or barrel-stave pore. In the barrel-stave model, the lipids are envisioned to stand upright around the peptides, allowing the peptides to interact with the core of the lipid bilayer. In the toroidal pore model, the lipids in each leaflet align themselves so that the lipid head groups line the outside of the pore. The evidence we have from the simulation more closely supports the barrel-stave model. Although we see clear evidence of the lipids reordering themselves to allow the head groups to interact with the turn and termini regions of the peptides, the lipids never move so as to completely line the pore with their head groups. This is in agreement with data from the NMR experiments by Mani and co-workers who noted that such a lining of the pore by lipid head groups contradicts ^{1}H spin diffusion data that show contact between the lipid chains and the peptides.[3] Additionally, one of the hypotheses of the toroidal pore model is that the peptides are monomeric.[56] We observe in the simulations that the dimers are intact throughout the simulation and that although interdimer pairs are not as tightly bound as intradimer pairs they do interact strongly with each other (data not shown). Furthermore, the peptides clearly interact with the lipid carbonyl chains with hydrophobic interactions during the length of the simulation. Therefore, we propose the barrel-stave model to explain the manner in which PG-1 forms pores in a bacterial membrane mimic. We should note that evidence has been mounting for both the barrel-stave and the torroidal pore model, but for different lipids and ion concentrations.[3,44,45,57] It is likely that there is no single, universal membrane structural character

(44) Tang, M.; Waring, A. J.; Hong, M. Phosphate-mediated arginine insertion into lipid membranes and pore formation by a cationic membrane peptide from solid-state NMR. *J. Am Chem Soc.* **2007**, *129* (37), 11438−11446.
(45) Tang, M.; Waring, A. J.; Hong, M. Trehalose-protected lipid membranes for determining membrane protein structure and insertion. *J. Magn. Reson.* **2007**, *184* (2), 222−227.
(46) Heller, W. T.; Waring, A. J.; Lehrer, R. I.; Harroun, T. A.; Weiss, T. M.; Yang, L.; Huang, H. W. Membrane thinning effect of the beta-sheet antimicrobial protegrin. *Biochemistry* **2000**, *39* (1), 139−145.
(47) Sokolov, Y.; Mirzabekov, T.; Martin, D. W.; Lehrer, R. I.; Kagan, B. L. Membrane channel formation by antimicrobial protegrins. *Biochim. Biophys. Acta* **1999**, *1420*, 23−29.
(48) Brelidze, T. I.; Niu, X.; Magleby, K. L. A ring of eight conserved negatively charged amino acids doubles the conductance of BK channels and prevents inward rectification. *Proc. Natl. Acad. Sci. U.S.A.* **2003**, *100*, 9017−9022.
(49) Cai, M.; Jordan, P. C. How does vestibule surface charge affect ion conduction and toxin binding in a sodium channel. *Biophys. J.* **1990**, *57*, 883−891.

adopted regardless of the nature of the lipids or the peptide, although the luxury of observing the full motion of lipids is only afforded to simulations.

PG-1 is only about 30 Å long, whereas the POPE:POPG membrane is approximately 45 Å thick. As a result, the lipids nearest the pore reorder in such a way as to allow the head groups to interact with the positively charged arginine groups while the hydrophobic residues interact with the lipid chains. This causes localized thinning of the membrane in agreement with lamellar X-ray diffraction measurements.[46]

Ion transport through the pore is directly related to AMP biological function. We demonstrate that the transmembrane pores formed by PG-1 would be able to contribute to a destabilization of the electrochemical potential gradient across the cell membrane due to their strong preference for transporting chloride ions over sodium ions across the bilayer. Presumably potassium ions will also be largely excluded from the pore (we are currently conducting simulations with other ion species to investigate the relative selectivity). We have shown that the arginine residues attract negatively charged chloride ions to the pore so that these ions pass through the pore easily. We note a slightly higher incidence of ions passing from the turn end to the termini end of the pore, although the observed difference may be an artifact of the small simulated sample. This nearly zero net flux of ions through the pore is due to the fact that there is no concentration gradient in our system. In a biologically relevant setting, there is a gradient of ionic species, which is necessary for the establishment of the transmembrane potential. This is in turn necessary to counter the osmotic pressure build-up because of the highly concentrated contents in the cytoplasm. A concentration gradient between the inside and outside of the cell would presumably have a noticeable effect on the net flux of negatively charged ions through the pore. This preference of the PG-1 pore to chloride ions is consistent with the experimentally observed anion selectivity of the PG-1 pore in phospholipid bilayers.[47] The selectivity of the PG-1 pore for anions is due to electrostatic interactions with the charged arginine residues located at both entrances of the pore. The increase of the concentration of the anions around the charged residues at both entrances increases the likelihood of transitions of these ions from one side to the other, a phenomenon that has been observed in several previous experimental and simulation studies of ion channels rich in charged residues.[48−52]

Strong ion−ion correlations and ion pairings have previously been shown to affect the permeation of ions in wide ion channels,[53] and in the PG-1 pore, similar effects are observed, especially for the passage of sodium ions through the pore.

A calculation of a theoretical limit to conductance values was possible with the measured diffusivities of molecular species through the pore. These are in agreement as an upper bound to the experimentally measured conductance: Lehrer and coworkers measured the conductance of PG-1 pores and found values ranging between 50 and 100 pS.[47] We should certainly stress that the simulated and experimental systems are not identical: The experimental measurements were taken at a bulk ionic strength of (KCl electrolyte) 100 mM, while in our simulation we used a bulk ionic strength of 150 mM (NaCl electrolyte). Also, it has been observed that the maximal conductance of Na^+ and K^+ ions depends on the composition of the lipid membrane.[43,58] The *I*−*V*/conductance experiments used an unspecified phospholipid mixture that forms "black lipid membranes",[47] different from the 3:1 POPC:POPG mixture in the simulation, which could also account for the discrepancy. Finally, a major assumption for the calculation of the maximum conductance according to eq 3 is that no more than one ion can simultaneously occupy the pore, which is not true for the protegrin pore. Nonetheless, we believe that the results are interesting enough to report. At the very least they provide motivation for additional exploration with nonequilibrium simulations and the application of external voltage.

We turn to the question of how does PG-1 actually kill bacterial cells? Is cell death due solely to transport of ions, or can osmotic lysis explain the antimicrobial activity of PG-1? We can conjecture that a protegrin pore can result in a gradual disappearance of the transmembrane potential, by allowing ions to flow through the membrane. The transmembrane potential is the result of the ion concentration gradient across the membrane that cells employ as a countermeasure to the hypertonic cytoplasmic environment. If the bacterial cells are surrounded by an extracellular host medium that has a lower osmolality than inside the cell, then the absence of the transmembrane potential will cause water to rush into the bacterial cell, swelling it, and causing its death.

The diffusion coefficient and PMF of water estimated here suggests that osmotic lysis after the decay of the transmembrane potential is a plausible explanation for the mechanism of action of PG-1. The diffusive water permeability across the PG-1 pore can be calculated by

$$P_{\mathrm{w}} = \frac{A_{\mathrm{pore}} D_{\mathrm{pore}}}{L_{\mathrm{pore}}} \tag{4}$$

where D_{pore} is the effective diffusion coefficient of water within the pore, A_{pore} is the effective cross section area of the pore, and L_{pore} is the length of the pore. The effective diffusion coefficient, the effective cross-section area of the pore and the length of the pore are assumed to be 0.1 Å^2/ps, 200 Å^2 and 30 Å, respectively. With these values, we calculate a lower bound for the single pore diffusive water permeability to be ap-

(50) Consiglio, J. F.; Andalib, P.; Korn, S. J. Influence of Pore Residues on Permeation Properties in the Kv2.1 Potassium Channel. Evidence for a Selective Functional Interaction of K+ with the Outer Vestibule. *J. Gen. Physiol.* **2003**, *121*, 111−124.
(51) Kienker, P.; Tomaselli, G.; Jurman, M.; Yellen, G. Conductance mutations of the nicotinic acetylcholine receptor do not act by a simple electrostatic mechanism. *Biophys. J.* **1994**, *66*, 325−334.
(52) Aubin, C. N. S.; Linsdell, P. Positive Charges at the Intracellular Mouth of the Pore Regulate Anion Conduction in the CFTR Chloride Channel. *J. Gen. Physiol.* **2006**, *128*, 535−545.
(53) Im, W.; Roux, B. Ions and counterions in a biological channel: a molecular dynamics simulation of OmpF porin from Escherichia coli in an explicit membrane with 1 M KCl aqueous salt solution. *J. Mol. Biol.* **2002**, *319*, 1177−1197.
(54) Yang, B.; Verkman, A. S. Water and Glycerol Permeabilities of Aquaporins 1−5 and MIP Determined Quantitatively by Expression of Epitope-tagged Constructs in Xenopus Oocytes. *J. Biol. Chem.* **1997**, *272*, 16140−16146.
(55) Sukharev, S. I.; Blount, P.; Martinac, B.; Blattner, F. R.; Kung, C. A large-conductance mechanosensitive channel in E. coli encoded by mscL alone. *Nature* **1994**, *368*, 265−268.
(56) Ludtke, S. J.; He, K.; Heller, W. T.; Harroun, T. A.; Yang, L.; Huang, H. W. Membrane pores induced by magainin. *Biochemistry* **1996**, *35*, 13723−13728.
(57) Tang, M.; Waring, A. J.; Hong, M. Phosphate-mediated arginine insertion into lipid membranes and pore formation by a cationic membrane peptide from solid-state NMR. *J. Am Chem Soc.* **2007**, *129*, 11438−11446.
(58) Roux, B.; Karplus, M. Ion Transport In a Gramicidin-like Channel: Dynamics and Mobility. *J. Phys. Chem.* **1991**, *95*, 4856−4868.

proximately 6.67×10^{-12} cm^3/s and water molecule turnover number of the pore to be approximately 2.2×10^{11} molecules/s. This estimate of the diffusive permeability of the PG-1 pore is 1−2 orders of magnitude higher than the $3.3-24 \times 10^{-14}$ cm^3/s of aquaporin channels.[54] The large diffusive permeability through PG-1 pores suggests that these pores cause a serious disruption to the ability of bacterial cells to control the flow of water using its native water selective channels. Hence, the osmotic water flow is an important factor in the destabilization of the bacterial membrane permeability, one which can lead to a quick cell death by osmotic lysis when bacterial cells are no longer able to slow down or prevent this process by protection mechanisms, such as those that have been found in *Escherichia coli* where mechanically sensitive channels become activated as a last resort.[55]

The simulation of an octameric assembly of PG-1 peptides in a POPE:POPG bilayer described in this work has provided detailed images of the interactions of the pore with the bilayer and of the movement of ions in the system. What we have observed leads us to propose that the PG-1 pore aggregates according to the barrel-stave model. We observe significant movement of negatively charged ions and water through the pore. As such, protegrin pores can effectively eliminate the cell's ability to regulate its osmolarity. We conjecture about how the permeability of water through the PG-1 pore is sufficient to cause cell death by osmotic lysis, although the actual mechanism of cell death is admittedly more complicated due to cellular protection mechanisms.

Acknowledgment. This work was supported by a grant from NIH (GM 070989). Computational support from the Minnesota Supercomputing Institute (MSI) is gratefully acknowledged. This work was also partially supported by National Computational Science Alliance under MCA04T033 and utilized the bigben cluster at the Pittsburgh Supercomputing Center. We thank R. Mani and Professors Mei Hong, Alan Waring and Robert Lehrer for providing us with the NMR model of the protegrin pore and for useful discussions.

Supporting Information Available: More data regarding the stability of the pore structure; discussion of the ion residence time distribution. This material is available free of charge via the Internet at http://pubs.acs.org.

JA0780380